J Solid State Electrochem (2010) 14:1333–1338
DOI 10.1007/s10008-009-0935-x

ORIGINAL PAPER

Electrochemical intercalation of O^{2-} in $CuAlO_2$ single crystal and photoelectrochemical properties

Razika Brahimi · Mohamed Trari · Aïssa Bouguelia · Yassine Bessekhouad

Received: 20 February 2009 / Revised: 10 September 2009 / Accepted: 13 September 2009 / Published online: 1 October 2009

Abstract The delafossite $CuAlO_2$ single crystal, prepared by the flux method, is a low mobility p-type semiconductor with a hole mobility of 1.2×10^{-5} cm^{-2} V^{-1} s^{-1}. The chronoamperometry showed an electrochemical O^{2-} insertion with a diffusion coefficient D_{303K} of 3.3×10^{-18} cm^2 s^{-1}. The thermal variation of D in the range 293–353 K gave an enthalpy of diffusion (ΔH) of 44.7 kJ mol^{-1}. $CuAlO_2$ is photoactive, and the Mott–Schottky plot indicates a flat band potential of +0.42 V vs saturated calomel electrode and a holes density (N_A) of 10^{16} cm^{-3}. The photocurrent spectra have been analyzed by using the Gartner model from which the absorption coefficients and diffusion lengths were determined. An optical transition at 1.66 eV, indirectly allowed, has been obtained. The spectral photoresponse provides a high absorption at 480 nm. The low quantum yield (η) is attributed to a small depletion length (440 nm) and a hole diffusion width (271 nm) compared to a very large penetration depth (12 μm).

Keywords Delafossite · $CuAlO_2$ · Single crystal · Oxygen intercalation · Diffusion · Photoelectrochemical

R. Brahimi
Centre of Research in Physical and Chemical Analysis (CRAPC), BP 248, RP 16004 Algiers, Algeria

R. Brahimi · M. Trari (✉) · A. Bouguelia · Y. Bessekhouad
Laboratory of Storage and Valorization of Renewable Energies, Faculty of Chemistry (USTHB), BP 32, 16111 Algiers, Algeria
e-mail: labosver@gmail.com

Introduction

There has been renewed interest in the last years on the materials which can be used in fuel cells and photoelectrochemical (PEC) devices [1]. So, the development of new electrodes for the conversion of incident photon to electrical power and/or chemical energy has been extensively motivated [2]. The delafossites $CuMO_2$, where M is commonly a trivalent metal, are thermodynamically stable phases of copper (I) oxide and have evolved rapidly from single crystal to thin solid films [3] passing by the ceramic powder [4]. They are promising for the solar energy conversion and environmental protection [5]. The flat band potential (E_{fb}) does not depend on pH, and consequently, the conduction band (CB) can be appropriately matched to electrolyte levels for photoinduced hydrogen evolution [6]. Attention would, therefore, be directed toward $CuAlO_2$ which was found as having the required energetic factors for PEC conversion, in addition to being chemically stable and low cost. Among the 3D metals, copper is by far the most attractive with regard to the chemical stability, and $CuAlO_2$ exhibits a corrosion rate smaller than 1 μmol m^2 $year^1$ [7]. The two-dimensional lattice presents an interest both from the basic and applied point of view. The structure is highly anisotropic and revealed infinite $_\infty[AlO_2]$ layers extending in the basal plans. So, an electrochemical oxygen insertion in the crystal lattice is expected. Such prediction has found an experimental support, and oxygen overstoichiometry has been reported in delafossites [8]. The thermodynamic favors the insertion of ions of comparable dimensions which has been shown to give phases for which the diffusion coefficient averages 10^{-15} cm^2 s^{-1} [9] and proceeds with relatively low activation energy. The experiments were performed in basic media where $CuAlO_2$ exhibits a high chemical stability, and the

chronoamperometric data were fitted according to finite diffusion model [10].

The stoichiometric oxide is expected to be insulating. Nevertheless, in delafossite, the transport properties are tailored by oxygen insertion in the Cu plans giving the opportunity for characterizing the oxide photoelectrochemically. However, whereas the semi conducting properties have given rise to some studies and interpretations, the PEC characterization of single crystal has not been subject of any previous investigation. In addition, some intrinsic properties can be evaluated only on the single crystal. With this in mind, we characterized $CuAlO_2$ single crystal by the photocurrent technique. In a previous paper, we reported the transport properties along with preliminary electrochemical properties [11]. In extension, the present work covers the intercalation of oxygen and diffusion properties. In a second part, we investigated the PEC characterization using the Gartner model.

Experimental

$CuAlO_2$ single crystals were obtained by the flux method with a slightly modified technique described in Ref. [12]. We have taken a mixture of $Cu2O/Al_2O_3$ (3/1) in molar ratio under argon atmosphere. The crystal growth was performed in a platinum crucible standing in a thermally controlled furnace at 1,160 °C. The cooling rate (1.5 °C/hr) was controlled from 1,140 to 700 °C below which the sample followed the natural cooling. The crystals appeared black mirror like in reflected light and have almost a hexagonal shape; they exhibit a blue color, and their length lies between 1 and 3 mm. The selected crystal was a hexagonal platelet with (001) main face and $2\times2\times0.2$ mm^3 size. The current contacts were made by painting silver paste onto the entire area of the crystal to ensure a uniform current injection. The linear domain of the current–voltage characteristic was checked. The conductivity was determined by the two probe method using a current of 1 mA. It was calculated from the relation $\sigma_\perp = Kj/V$, where K is a form factor determined from the geometry of crystal and the position of the probes. The temperature was measured with a digital-calibrated thermocouple (type K).

In–Ga back contacted (001)-oriented crystals were made, and the crystals were mounted in glass holders with insulating epoxy. The electrochemical measurements were done in a double-walled cell whose temperature was regulated by a thermostated bath (Julabo). High purity platinum (Tacussel, 5N) served as auxiliary electrode and $Hg/HgCl_2$/sat KCl (SCE) as reference electrode. The potential of the working electrode (WE) was monitored by a Voltalab PGZ 301 potentiostat. The interfacial capacitance has been determined as a function of the potential with a rate of 10 mV $step^{-1}$. Alternating current (AC) voltage signal of 10 kHz in frequency, and 10 mV peak to peak in magnitude was applied to the system. The KOH (1 M) solution was continuously purged of air by bubbling through with nitrogen. For the electrochemical oxygen insertion, high impedance boxes (AOIP) was employed for the intentiostatic mode. The photocurrent spectrum has been measured when WE was biased at −0.4 V. The electrode was irradiated through a flat window by a 650-W Xenon lamp (Dyr) whose output was passed through a monochromator with 10 nm bandpass. The light intensity was measured at each wavelength (λ) with a flux meter (Testo 545) positioned at the same position of WE.

Results and discussion

$CuAlO_2$ crystallizes in the delafossite structure and occurs mainly in the polytype 3R (space group: $R\bar{3}m$, D^5_{3d}). The X-ray diffraction pattern showed a hexagonal unit cell, and the lattice constants: a=0.2852 nm and c=1.6944 nm, determined on ground crystals, agree with the literature [12]. The structure can be visualized as close-packed layers of Al^{3+} octahedra sharing common edges. The layers are linked to each other by linear CuO_2^{3-} "dumb-bell" units parallel to c-axis, and in which, oxygen, in sp^3 hybridized state, is tetrahedrally coordinated by three Al^{3+} and one Cu^+. The $(AlO_6)_\infty$ layers are sandwiched between Cu monolayer giving $CuAlO_2$ anisotropic properties. The Al^{3+} ions form triangular sublattices stacked along the (001) direction in a three-layer repeat sequence ABCABC. The Cu–O distance (0.1835 nm) is in perfect agreement with the sum of ionic radii, $^{II}Cu^+$ (0.046 nm) and $^{IV}O^{2-}$ (0.138 nm) [13] and confirms the ionicity of the bond, II and IV are the coordination numbers.

The a parameter, equal to the average Cu^+–Cu^+ distance within the layers, is relatively longer and consistent with the semiconducting behavior. The (001) plan, where the electrical conductivity $\sigma_\perp$ is by two orders greater than that along the c-axis, has been used as active surface area. $\sigma_{\perp 300K}\left(=5.7\times10^{-7}\Omega^{-1}cm^{-1}\right)$, measured by the two probe technique with knowledge of the crystal cross-sectional area, agrees with the band diagram reported early by Rogers et al. [14]. The band edges are defined by the d levels splitting of Cu(I) in the linear field. The lower, filled levels (d_{xz} and d_{yz}) providing the valence band (VB), though being nonbonding whereas CB consists of empty hybridized Cu^+: d_{z2}-s).

Ions intercalation in the low dimensional lattices, where the geometric constraints are easily relieved, offers unexplored ways for the synthesis of new phases not accessible by solid state reaction. The ease of insertion in delafossites may be understood in terms of

interconnected channels of sufficient size to allow oxygen transport.

The intensity potential $j(E)$ characteristic was plotted in KOH as indifferent electrolyte owing to its high electroconductivity (Fig. 1), the current is nearly zero over a wide potential range. Anodic potential gives rise to oxidation of the crystal with a peak (A, −0.30 V, j_{ox} ~0.01 mA cm^{-2}) lower than that corresponding to O_2 evolution, based on:

$$CuAlO_2 + 2\delta\ OH^- \rightarrow CuAlO_{2+\delta} + \delta\ H_2O + 2\ \delta e^- \qquad (1)$$

where δ stands for the amount of intercalated oxygen. This potential corresponds, in the Pourbaix diagram [15], to potentials of theoretical equilibria which are concerned with hydrated oxides of Cu^{II}. As noticed above, the Cu^+–Cu^+ distance is large enough to accommodate oxygen electrochemically and is achieved by an internal redox process $Cu^{+/2+}$ to maintain the charge neutrality. On the reverse scan, the cathodic peak (R, −1.05 V) completely desintercalates the oxygen from the lattice. A fast electron transfer is characterized by a separation between the oxidation and reduction peaks of 0.06/m. However, the large difference (~0.7 V) indicates a low oxygen insertion/desinsertion, m being the number of exchanged electrons.

Below −1.1 V, the current increases steeply due to H_2 liberation. On the contrary, the large overvoltage in the anodic region which exceeds 1 V indicates a low electro catalytic activity of $CuAlO_2$ with regard to oxygen evolution. The electrochemical oxidation is a powerful technique of producing oxygen enrichment in the layered compounds. The coulometric titration was performed in intentiostatic mode (low intensity) to preclude parasitic oxidations and to

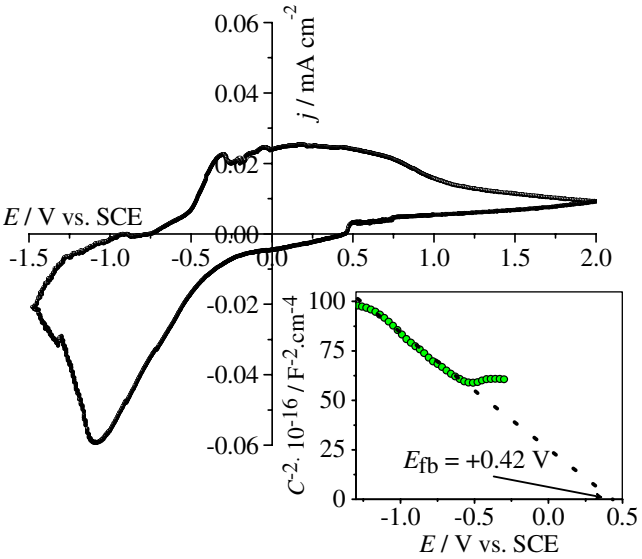

Fig. 1 Potentiodynamic $j(E)$ profile of $CuAlO_2$ single crystal in 1 M KOH under N_2 bubbling, scan rate 2.5 mV s^{-1} at 302 K. The Mott–Schottky characteristic plotted at a frequency of 10 kHz (*inset*)

have a current efficiency close to 100%. Thus, an anodic current of 1 mA was maintained during 96 h. It is helpful to mention that the crystal after polarization exhibits a positive thermopower (980 μV K^{-1}), an evidence of oxygen intercalation. It indicates that the majority carriers are of p type, suggesting the conduction mechanism to be predominantly by holes hopping. The oxygen overstoichiometry is calculated from the overall charge transfer assuming the O^{2-} formation. By passing a charge of ~9 C through the cell, the δ value is determined to be 0.028. The free potentials at zero current, measured before (−0.160 V) and after electrochemical oxidation (−0.029 V), can be correlated to the Fermi level (E_f) which is an intrinsic characteristic of the oxide. This suggests that when $CuAlO_2$ is oxidized, electrons are coming out from the copper plans and lowers the energy E_f. The oxygen inserts reversibly, and the diffusion current j_{dif} as a function of time is given by [10]:

$$j_{dif} = neFSD\left(\frac{\partial C}{\partial x}\right)_{x=1} = j_{\mathrm{dif}}$$
$$= \frac{neFSD2C_0}{l}\sum_{i=0}^{i=11}\left\{\frac{D\pi^2(2i+1)^2 t}{4l^2}\right\} \qquad (2)$$

where n is the oxidation state of O^{2-} (= 2), S is the active surface (0.025 cm^2), t is the time, and C_o is the density of Cu^+ ions (2.51×10^{22} cm^{-3}). Taking three coppers per unit cell, C_o corresponds to a concentration 0.415 mol cm^{-3}. The chronoamperometry was performed at various potentials, and the mathematical correlation of the model provides the value of the adjustable parameters, i.e., the diffusion coefficient D (3.3×10^{-18} cm^2 s^{-1}) and the diffusion length l (0.39 nm). The full lines, fitted up to i=11, represent the theoretical model whereas the dashed lines give the corresponding experimental data (Fig. 2). The discrepancy for the potential 0.7 V is due to the further oxidation of copper ($Cu^{2+/+3}$) [16]. The thermal variation of D was investigated for the best potential (−0.2 V). As expected, the diffusion increases with increasing temperature and reveals that the progress is endothermic. This is consistent with previous work on $CuLa_2O_4$ where D was found to be 2.5×10^{-16} cm^2 s^{-1} at 298 K [17]. The plot of (ln D) against reciprocal temperature obeys an Arrhenius type law:

$$D = D_0 \exp\left[-\frac{\Delta H}{RT}\right] \qquad (3)$$

The relatively low diffusion enthalpy (ΔH) value (44.7 kJ mol^{-1}), calculated from the slope (Fig. 3), shows that the channels in the basal plans are involved in the oxygen diffusion and clearly evidences the high mobility of oxygen in the delafossite framework. Such a migration needs diffusion path within the parent structure which exist along the (100) and (010) directions, easily seen in the crystal

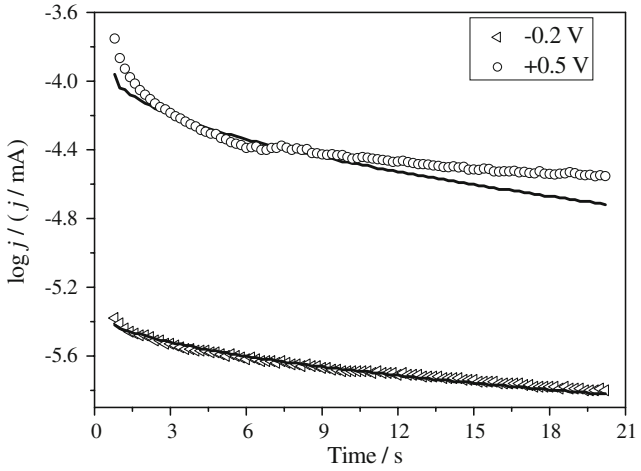

Fig. 2 The anodic transient currents of $CuAlO_2$ single crystal in 1 M KOH under N_2 bubbling (*dashed lines*). *Full lines* represent the finite diffusion model

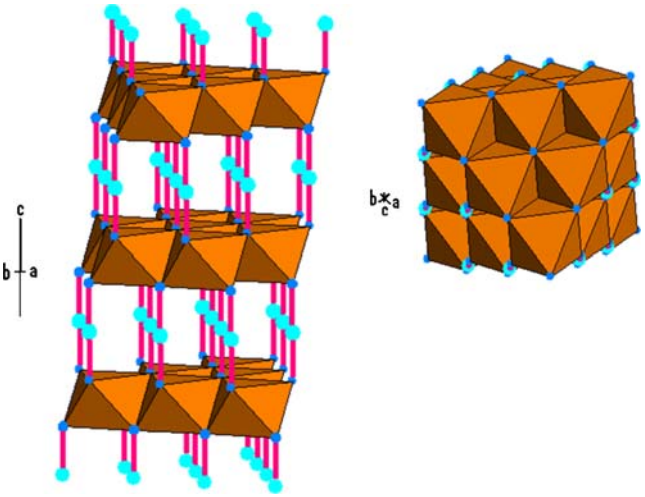

Fig. 4 Delafossite type structure of $CuAlO_2$ showing the two-dimensional character with the corresponding channels. *Big circles* represent Cu^+ located between layers of AlO_6 octahedra. Projection on the (001) plan (*right*)

structure (Fig. 4). The plot is linear, but when increasing the temperature, it deviates with a marked departure from the straight line showing the nonvalidity of the model at high temperature.

The exchange of majority charge carriers between $CuAlO_2$ and the electrolyte occurs in a direct way where the diffuse charge in the space charge region together with its countercharge in the Helmholtz layer are approximated by a plate condensator. To evaluate the semiconducting properties, the Mott–Schottky characteristic was plotted at a frequency of 10 kHz:

$$\frac{1}{C^2} = \pm\frac{2}{e\varepsilon\varepsilon_0 S N_A}\left(E - E_{fb} - \frac{kT}{e}\right) \quad (4)$$

where ε and ε_o are, respectively, the dielectric constants of the oxide and vacuum (8.85×10^{-14} F cm^{-1}), E is the applied potential, e is the elementary charge, and kT is the thermal energy which averages 25 mV at room temperature. The sign ± is relative to n or p type. The curve, depicted in Fig. 1 (inset), shows a linear behavior from which a flat band potential (E_{fb}) of +0.42 V, and a holes density (N_A) of 10^{16} cm^{-3} were determined, respectively, from the intercept to $C^{-2}=0$ and the slope. The negative slope lends a further support of p type character of $CuAlO_2$, attributed to oxygen insertion. For a semiconductor, the electro affinity (χ) is related to the potential E_{fb} by the empirical relation:

$$\chi = eE_{fb} + 4.75 + \Delta E \quad (5)$$

ΔE being the activation energy (= 0.32 eV) [11]. The calculated χ value (5.5±0.1 eV) is typical of oxides in which CB derives mainly from Cu: 3D orbital [18].

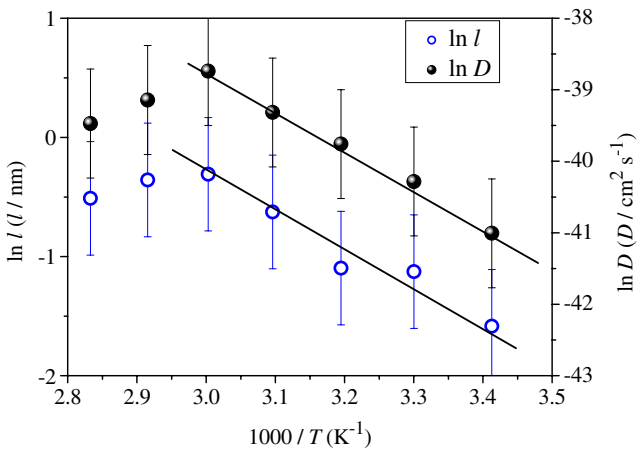

Fig. 3 The thermal variation of the diffusion coefficient (D) and the diffusion length (l)

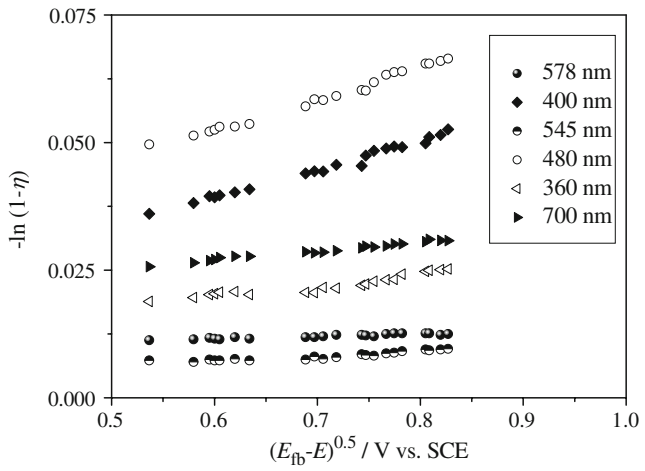

Fig. 5 Plots of $-\ln(1-\eta)$ vs $(E_{fb}-E)^{0.5}$ for the determination of semiconducting properties of $CuAlO_2$ single crystal

Table 1 Physical parameters of $CuAlO_2$ single crystal

λ (nm)	ξ ($\pm\Delta\xi$; cm^{-1})	$10^3\times\xi^{-1}$ (cm)	L_D (nm)	$W+L_D$ (nm)
360	838 (±5.4)	1.19	679.3	1,119.3
400	796 (±5.0)	1.26	126.3	566.3
480	840 (±4.6)	1.19	271.4	711.4
545	145 (±2.0)	7.08	143.4	583.4
578	74.3 (±1.3)	13.00	1,164	1,604.0
700	0.124 (±0.1)	5.73	1,200.5	1,640.5

It is of interest to discuss briefly the origin of optical transitions in $CuMO_2$ in terms of band structure. In delafossite, the transitions are of *d–d* character, belonging to the visible region, and are governed mainly by the Cu–O bond [14]. Cu^+ is linearly coordinated, and only one type of charge transfer ($Cu^+\rightarrow Cu^+$) can be involved in the energy range considered. The charge transfer O^{2-}: $2p\rightarrow Cu^+$: 3D occurs at energies higher than 4 eV and cannot be observed owing to the low lying O^{2-}: 2p orbital [19]. The highest occupied molecular orbital and the lowest unoccupied molecular orbital are predominantly Cu 3D orbital in character with a separation characterized by the strength of the ligand field. CB of hybridized 4s/3D orbital is separated from VB by a gap (E_g) of ~2 eV. The ion M^{3+} undoubtedly plays an important role in the band diagram, and aluminum allows the extension of the spectral photoresponse to lower photon energies. VB, arising from nonbonding orbital t_{2g}, lies approximately at the same energy regardless the nature of the ion M^{3+}. The relatively weak hybridization of Al–O lowers the antagonist antibonding band Cu–O toward small energies and decreases the gap (see below).

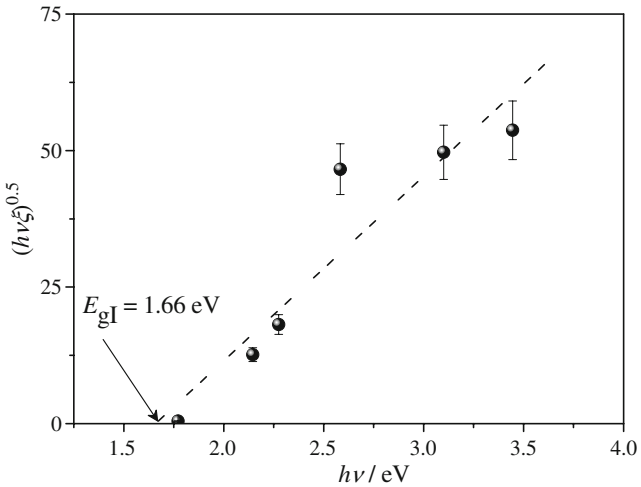

Fig. 6 Determination of the indirect allowed optical gap at 1.66 eV

There is a need to make an in-depth study to explain the low quantum efficiency (η) in $CuMO_2$. The space charge region is given by:

$$W=\left\{\frac{2\varepsilon\varepsilon_0(E_{fb}-E)^{0.5}}{eN_A}\right\} \tag{6}$$

For a band bending (E_{fb}–E) of 0.5 V, the depletion width (W) is found to be 440 nm. η, measured with monochromatic light, was determined by dividing the electron flow in the external circuit (from the photocurrent j_{ph}, subtracted from the dark current j_d) by the incident photon flux determined at each wavelength:

$$\eta=\frac{j_{ph}-j_d}{e\varphi} \tag{7}$$

Φ being the light power intensity falling on the electrode. The photocurrent–wavelength spectrum can be analyzed to get both the energy and type of interband transitions. When the rate-determining step in PEC process is the appearance of electrons at the interface, η is given by [20]:

$$\eta=1-\frac{\exp(-\xi W)}{1-\xi L_D} \tag{8}$$

L_D being the minority carrier diffusion width. The electrode was biased at −0.8 V, a value belonging to the plateau region in the $j_{ph}(E)$ curve. η is proportional to the absorption coefficient (ξ) if both the quantities ξW and $\xi L_D \ll 1$. Combining the Eqs. 4 and 6, one obtains:

$$-\ln(1-\eta)=\xi\left\{\frac{2\varepsilon\varepsilon_0}{eN_A}\right\}^{0.5}[E_{fb}-E]^{0.5}+\ln(1+\xi L_D) \tag{9}$$

From the linear part of $-\ln(1-\eta)$ against $(E_{fb}-E)^{0.5}$, illustrated in Fig. 5, the parameters ξ and L_D (Table 1) have been determined, respectively, from the slope and the intercept to zero *x*-axis. At low potential, the plot is linear, but when approaching the potential E_{fb}, it deviates from the straight line suggesting the inapplicability of the Gartner model at low band bending because the easy recombination process of electron per hole (e^-/h^+) pairs. The small diffusion widths L_D are understood in term of low mobility μ (1.2×10^{-5} cm^{-2} V^{-1} s^{-1})[1] where the carriers move in narrow electronic bands deriving from Cu 3D character. The optical absorption for interband transitions in a crystallized semiconductor close to the band energy varies as:

$$(h\nu\xi)^{0.5}=A(h\nu-E_g) \tag{10}$$

[1] *Calculated from the relation* $\sigma=\mu eN_A$.

The intercept of the linear plot of $(h\nu\xi)^{0.5}$ with the $h\nu$-axis (Fig. 6) yields E_g value of 1.66 eV, close to that given by others [19], and the transition is indirectly allowed, $h\nu$ being the incident photon. It is known that the recombination of (e^-/h^+) pairs predominates when the space charge region (W) is smaller than the length L_D. At λ_{max} (480 nm), the penetration depth (ξ^{-1}) reaches a length of 12 μm inside the crystal. This indicates that 94% of the pairs (e^-/h^+) are generated in the bulk, 3.7% in the space charge region, and only 2.3% in the diffusion width. These calculations explain, at least partially, the low quantum yields obtained with $CuMO_2$ [21].

Conclusion

$CuAlO_2$ single crystal was grown by the flux method. Cu^{2+} is generated by oxygen insertion to maintain the electroneutrality, and the oxide exhibited p-type conductivity. Chronoamperometric experiments showed oxygen intercalation in the layered lattice where the channel in the basal plans are involved for the diffusion process. The enthalpy of the diffusion has been determined. Aluminum extends the light absorption toward the visible region. The analysis of the photocurrent spectrum revealed an indirect energy band gap, due to Cu–Cu transition. The semiconducting properties have been investigated by the AC impedance whereas the relation between the photocurrent and applied potential has been analyzed by the Gartner model

Acknowledgment This study is supported by the Centre and the Faculty of Chemistry (C.R.A.P.C. Algiers). The authors greatly acknowledge Dr. Z. Lehanine for her valuable advices in the programmation of the theoretical model and Prof. A. Benchettara for capacitance measurements.

References

1. Brahimi R, Bessekhouad Y, Bouguelia A, Trari M (2007) Catal Today 122:62
2. Derbal A, Omeiri S, Bouguelia A, Trari M (2008) Int J Hydrogen Energy 33:4282
3. Banerjee AN, Kundoo S, Chattopadhyay KK (2003) Thin Solid Films 440:5
4. Shy JH, Tseng BH (2005) J Phys Chem Solids 66:2123
5. Omeiri S, Gabes Y, Bouguelia A, Trari M (2008) J Electroanal Chem 614:31
6. Brahimi R, Bessekhouad Y, Bouguelia A, Trari M (2007) J Photochem Photobiol A 186:242
7. Koriche N, Bouguelia A, Aider A, Trari M (2005) Int J Hydrogen Energy 30:693
8. Zhao T-R, Hasegava M, Takei H (1997) J Crystal Growth 181:55
9. Grenier JC, Doumerc JP, Muraoka Y, Petit S, Pouchard M, Wattiaux A (1998) Solid State Ionics 108:9
10. Crank J (1975) The mathematics of diffusion. Clarendon, Oxford
11. Brahimi R, Bellal B, Bessekhouad Y, Bouguelia A, Trari M (2008) J Cryst Growth 310:4325
12. Ishiguro T, Kitazawa A, Mizutani N, Kato M (1981) J Solid State Chem 40:170
13. Shannon RD (1976) Acta Crystallogr A32:751
14. Rogers DB, Shannon RD, Prewitt CT, Gillson JL (1971) Inorganic Chemistry 10:723
15. Pourbaix M (1963) Atlas d'équilibres électrochimiques. Gauthiers-Villards, Paris
16. Grenier JC, Wattiaux A, Lagueyte N, Park JC, Marquestaux E, Etourneau J, Pouchard M (1991) Physica C 173:139
17. Sanchez RD, Torresi RM, Rettori C, Oseroff S, Fisk Z (1994) Electrochim Acta 40:209
18. Trari M, Bouguelia A, Bessekhouad Y (2006) Sol Energy Mater & Sol Cells 90:190
19. Robertson J, Peackock PW, Towler MD, Needs R (2002) Thin Sold Films 411:96
20. Xia SJ, Zhou WF (1995) Electrochim Acta 40:175
21. Saadi S, Bouguelia A, Trari M (2006) Sol Energy 80:272